frontiers | Frontiers in Endocrinology

TYPE Original Research
PUBLISHED 08 March 2023
DOI 10.3389/fendo.2023.990078

OPEN ACCESS

EDITED BY
Zhi-Feng Sheng,
Second Xiangya Hospital, Central South University, China

REVIEWED BY
Dominik Saul,
Mayo Clinic, United States
Dongdong Qin,
Yunnan University of Chinese Medicine, China

*CORRESPONDENCE
Zhixiang Liu
lzxdff688@163.com
Hui Ren
renhuispine@163.com
Xiaobing Jiang
spinedrjxb@sina.com

†These authors have contributed equally to this work

SPECIALTY SECTION
This article was submitted to Bone Research, a section of the journal Frontiers in Endocrinology

RECEIVED 09 July 2022
ACCEPTED 30 January 2023
PUBLISHED 08 March 2023

CITATION
Zhang P, Chen H, Xie B, Zhao W, Shang Q, He J, Shen G, Yu X, Zhang Z, Zhu G, Chen G, Yu F, Liang D, Tang J, Cui J, Liu Z, Ren H and Jiang X (2023) Bioinformatics identification and experimental validation of m6A-related diagnostic biomarkers in the subtype classification of blood monocytes from postmenopausal osteoporosis patients.
Front. Endocrinol. 14:990078.
doi: 10.3389/fendo.2023.990078

Bioinformatics identification and experimental validation of m6A-related diagnostic biomarkers in the subtype classification of blood monocytes from postmenopausal osteoporosis patients

Peng Zhang[1,2†], Honglin Chen[1,2,3†], Bin Xie[1†], Wenhua Zhao[1,2], Qi Shang[1,2], Jiahui He[1,2], Gengyang Shen[3], Xiang Yu[3], Zhida Zhang[3], Guangye Zhu[1], Guifeng Chen[1,2], Fuyong Yu[1,2], De Liang[3], Jingjing Tang[3], Jianchao Cui[3], Zhixiang Liu[4*], Hui Ren[2,3*] and Xiaobing Jiang[2,3*]

[1]Guangzhou University of Chinese Medicine, Guangzhou, China, [2]Lingnan Medical Research Center of Guangzhou University of Chinese Medicine, Guangzhou, China, [3]The First Affiliated Hospital of Guangzhou University of Chinese Medicine, Guangzhou, China, [4]Affiliated Huadu Hospital, Southern Medical University, Guangzhou, China

Background: Postmenopausal osteoporosis (PMOP) is a common bone disorder. Existing study has confirmed the role of exosome in regulating RNA N6-methyladenosine (m6A) methylation as therapies in osteoporosis. However, it still stays unclear on the roles of m6A modulators derived from serum exosome in PMOP. A comprehensive evaluation on the roles of m6A modulators in the diagnostic biomarkers and subtype identification of PMOP on the basis of GSE56815 and GSE2208 datasets was carried out to investigate the molecular mechanisms of m6A modulators in PMOP.

Methods: We carried out a series of bioinformatics analyses including difference analysis to identify significant m6A modulators, m6A model construction of random forest, support vector machine and nomogram, m6A subtype consensus clustering, GO and KEGG enrichment analysis of differentially expressed genes (DEGs) between different m6A patterns, principal component analysis, and single sample gene set enrichment analysis (ssGSEA) for evaluation of immune cell infiltration, experimental validation of significant m6A modulators by real-time quantitative polymerase chain reaction (RT-qPCR), etc.

Results: In the current study, we authenticated 7 significant m6A modulators *via* difference analysis between normal and PMOP patients from GSE56815 and GSE2208 datasets. In order to predict the risk of PMOP, we adopted random forest model to identify 7 diagnostic m6A modulators, including FTO, FMR1,

YTHDC2, HNRNPC, RBM15, RBM15B and WTAP. Then we selected the 7 diagnostic m6A modulators to construct a nomogram model, which could provide benefit with patients according to our subsequent decision curve analysis. We classified PMOP patients into 2 m6A subtypes (clusterA and clusterB) on the basis of the significant m6A modulators *via* a consensus clustering approach. In addition, principal component analysis was utilized to evaluate the m6A score of each sample for quantification of the m6A subgroups. The m6A scores of patients in clusterB were higher than those of patients in clusterA. Moreover, we observed that the patients in clusterA had close correlation with immature B cell and gamma delta T cell immunity while clusterB was linked to monocyte, neutrophil, CD56dim natural killer cell, and regulatory T cell immunity, which has close connection with osteoclast differentiation. Notably, m6A modulators detected by RT-qPCR showed generally consistent expression levels with the bioinformatics results.

Conclusion: In general, m6A modulators exert integral function in the pathological process of PMOP. Our study of m6A patterns may provide diagnostic biomarkers and immunotherapeutic strategies for future PMOP treatment.

KEYWORDS

postmenopausal osteoporosis, RNA N6-methyladenosine (m6A) modulators, subtype classification, risk prediction, experimental validation

Introduction

Postmenopausal osteoporosis (PMOP) is a common bone disorder associated with ageing occurring in postmenopausal women, which is resulted from bone mass decrease and structural changes in bone tissue due to estrogen deficiency, resulting in increased bone fragility and susceptibility to fracture, as well as pain, bone deformation, comorbidities and even death caused by fracture (1–3). It is reported that approximately 50% of women experience at least one PMOP-related fracture (4). Existing drugs including vitamin D, calcium, denosumab, teriparatide, and bisphosphonates serve as recommended therapies for the treatment of PMOP (5), but long-term use of them trigger some side effects causing rapid bone loss and increasing the risks of the jaw osteonecrosis, atypical femoral fractures, and multiple rebound-related vertebral fractures (6). Therefore, PMOP still remains clinically not well managed (7). PMOP seriously impacts the health and life quality of the elderly and even shortens their life expectancy, increasing the financial and social burden on the countries and the families (8). Therefore, it is indispensable and critical to early identify patients at high risk of developing PMOP. Mounting evidence on the extensive developments in PMOP research shows that PMOP is a complicated disease of great heterogeneity that involves genetic changes (9). Hence, early identification and effective prevention of high-risk patients from a genetic perspective will exert a profound influence on the epidemiological control of PMOP.

Notably, recent studies have reported the promise of exosomes as potential therapies in osteoporosis (10, 11). Exosomes are small single-membrane organelles between 40 and 160 nm in diameter (12), which can carry a variety of cargos, such as lipids, proteins, glycoconjugates, and nucleic acids (13). Exosomes can transmit signals or molecules between cells and reshape the extracellular matrix by releasing these substances (14). Moreover, exosome can carry circular RNAs (circRNAs) to regulate bone metabolism in PMOP *via* sponging microRNAs (miRNAs), which can control mRNA expression by regulate the interaction with m6A methylation (15). N6-methyladenosine (m6A) is a widespread epigenetic modification that affects the variable splicing, translocation, translation and degradation of mRNA, as well as the epigenetic effects of certain non-coding RNAs (16). As an essential epigenetic modification, m6A modification needs numerous regulatory proteins encoded by writers, erasers, and readers to coorperate together (17). Abnormalities in m6A methylation can lead to a variety of diseases such as obesity, glioblastoma, acute myeloid leukaemia, type 2 diabetes, infertility, neuronal diseases, premature ovarian failure and various malignancies (18, 19). With the further study on m6A, researchers also found that bone marrow mesenchymal stem cells (BMSCs), chondrocytes, osteoblasts, osteoclasts, osteosarcoma, and adipocytes cells are all subject to m6A modification to regulate the methylation of RNA in cells, affecting the transduction of mRNA and/or non-coding RNA associated genes, thus activating cellular signaling pathways and affecting cell cycle and DNA damage repair, which in turn determines the occurrence and development process of musculoskeletal disorders (20–24). Recently, existing researches have verified that m6A modifications exert vital functions on the pathology of PMOP *via* modulating the expression level of m6A-associated genes (25, 26). However, it still stays unclear on the roles of m6A modulators derived from serum exosome in PMOP.

In this study, we performed a comprehensive evaluation on the roles of m6A modulators in the diagnostic biomarkers and subtype identification of PMOP on the basis of GSE56815 and GSE2208 datasets with monocyte samples. We developed a PMOP susceptibility prediction gene model based on seven candidate m6A modulators including FMR1, FTO, WTAP, YTHDC2, HNRNPC, RBM15 and RBM15B, and found that the model provided good clinical benefits for patients. Our RT-qPCR experiments further validated these m6A modulators, exhibiting consistent expression levels with the bioinformatics results. Additionally, we excavated two different m6A patterns that were closely correlated with immature B cell, gamma delta T cell, CD56dim natural killer cell, monocyte, neutrophil and regulatory T cell immunity, indicating that m6A patterns may be used to identify PMOP and provide subsequent treatment strategies. Figure 1 displayed the flowchart of study design and process.

Materials and methods

Sample retrieval

We collected monocyte samples separated from whole blood of elderly women by retrieving the GEO database (http://www.ncbi.nlm.nih.gov/geo/). The search terms were "BMD", "Postmenopausal Osteoporosis", "Gene expression", "Microarray", and the datasets were based on the following criteria: (1) each dataset includes at least 10 samples; (2) each dataset includes at least 5 cases in the groups of control and PMOP respectively; and (3) Both raw data and series matrix file can be obtained from the GEO datasets. Two datasets, GSE56815 (27) and GSE2208 (28) were eventually screened, which fully met our criteria. We chose 5 cases of control group and 5 cases of PMOP group from the dataset of GSE2208 as well as 20 cases of PMOP and 20 controls in GSE56815 dataset for subsequent analysis. Table 1 showed specific information of the corresponding datasets.

Data acquisition

We downloaded the annotated R package *via* Bioconductor (http://bioconductor.org/) to convert microarray probes to symbols in R (v4.1.2) software (Statistics Department of the University of Auckland, New Zealand). After data preparation, we carried out consolidation of the two datasets *via* SVA batch difference processing of combat and obtained the final dataset which contained 25 controls and 25 PMOP cases. Differential m6A madulators were identified from the dataset by difference analysis of control and PMOP cases using the R package of Limma. The screening thresholds to determine the significant m6A madulators were *P*-Value <0.05 and $|\log_2$ fold change (FC)$|$ >0 (29).

Model construction

We established random forest (RF) and support vector machine (SVM) models as training models to evaluate the PMOP occurrence, which were detected by "Reverse cumulative distribution of residual", receiver operating characteristic (ROC) curve, and "Boxplots of residual". In RF model, we used the R package of "RandomForest" to build an RF model to screen candidate m6A modulators with importance score (Mean Decrease Gini)>2. In SVM model, n stands for the number of m6A modulators and every data dot is presented as a dot in an n-dimensional space. We then selected an optimal hyperplane that distinguishes these two groups of control and PMOP very well (30). We then used the R package of "rms" to establish a nomogram model to

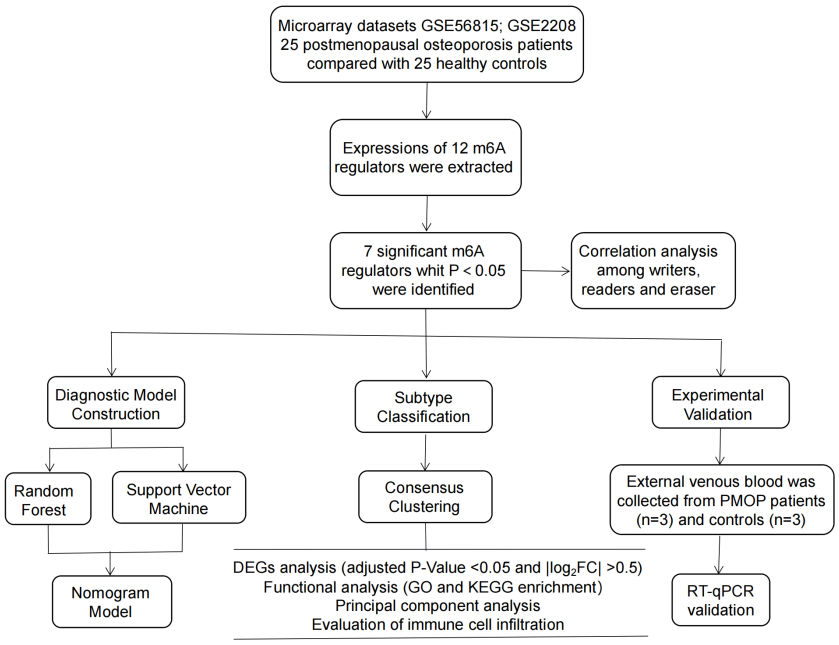

FIGURE 1
Flow chart of the study design.

TABLE 1 Information for the selected microarray datasets.

GEO Accession Total samples	Selected samples Platform	Source tissue
19 samples	10 samples	blood monocytes
GSE2208 Sample types:	GPL96 Sample types:	
10 high BMD	5 PreH BMD (Control)	
9 low BMD	5 postL BMD (PMOP)	
80 samples	40 samples	blood monocytes
GSE56815 Sample types:	GPL96 Sample types:	
40 high BMD	20 PreH BMD (Control)	
40 low BMD	20 postL BMD (PMOP)	

BMD, bone mineral density; PreH BMD: Premenopausal High BMD; postL BMD: Postmenopausal Low BMD.

predict the prevalence of PMOP patients according to screened candidate m6A modulators. We utilized the calibration curve to assess how well our predicted values align with reality. We also carried out decision curve analysis (DCA) to draw a clinical impact curve and assess whether decisions based on the model produced benefit to patients (31).

Subtype classification

Consensus clustering is a resampling-based algorithm that identifies each member and its subcluster number, and verifies the rationality of the clusters (31). Using the R package of "ConsensusClusterPlus", a consensus clustering method was conducted to identify different m6A patterns on the basis of significant m6A moderators (32).

Classification of differentially expressed genes between different m6a patterns and GO and KEGG enrichment analysis

We utilized Limma package to identify differentially expressed genes (DEGs) between different m6A patterns with the threshold of adjusted *P*-Value <0.05 and $|\log_2 FC| > 0.5$. Next, we used the R package of "clusterProfiler" to perform GO and KEGG analyses so as to investigate the possible mechanism of the DEGs involved in PMOP (33).

Calculation of the m6A score

We utilized principal component analysis to calculate the m6A score for each sample for quantification of the m6A patterns, with the m6A score evaluated based on the following formula: m6A score = $PC1_i$, where PC1 denotes principal component 1, and i denotes significant m6A gene expression (34).

Evaluation of immune cell infiltration

We utilized single sample gene set enrichment analysis (ssGSEA) to evaluate the level of immune cell infiltration in the samples from PMOP groups. First, the gene expression levels in the samples were sequenced using ssGSEA to obtain a ranking of gene expression levels. Next, we searched for the significant m6A madulators in the input dataset and then summed their expression levels. According to these evaluations, we obtained the abundance of immune cells in each sample (35).

Experimental validation by RNA extraction and real-time quantitative polymerase chain reaction

The clinical experiments involved in this paper were authorized by the Ethics Committee of the 1st Affiliated Hospital of GZUCM (No. K [2019]129). In the current research, all patients who participated in this trial provided informed consent at the beginning. Then, external venous blood was drawn from PMOP patients (n=3) and healthy controls (n=3) respectively. The two groups were age-matched. The manipulation of human peripheral blood monocytes (HPBMs) was performed as described previously (36). First, whole blood from patients was put into a 50-mL centrifuge tube, then diluted with 10-mL PBS and gently mixed. Afterwards, we continuously centrifuged the initial blood specimen at 2000 rpm for 20 minutes. When centrifugation was finished, the blood sample was stratified and the leukocyte layer in the center of the sample containing HPBMs was aspirated by pipette and transferred to a single fresh 15 mL centrifuge tube in liquid with 10-15 mL of PBS. Next the solution was centrifuged at 1500 rpm in 10 min and the supernatant was lifted to precipitate and be the wanted HPBMs. HPBMs were inoculated in 6-well plates, and then 1mL of TRIzol reagent was applied to each well for total RNA extraction from the cells. Subsequently, retrotranscription of 1μg of total RNA was done using a cDNA synthesis kit (Takara Inc.Shiga, Japan). 20μL SYBR Green qPCR SuperMix (Takara Inc.) was used for detection of m6A cDNAs and RT-qPCR machine (Bio-Rad, Hercules, CA, USA). The thermal cycling conditions for the final gene amplification were: 95°C for 30s, 40 cycles of 95°C for 5s, and a final step of 60°C for 30s. Quantitative analysis was performed using the $2^{\Delta\Delta CT}$ method to calculation of the relative expression of each gene. The gene-related detection primers of m6A modulators were compounded by Shanghai Sangon Biotechnology Co.Ltd (China), as shown in Table 2.

10.3389/fendo.2023.990078

Statistical analysis

The correlations among writer, reader and eraser were evaluated *via* linear regression analyses. The differences between groups were calculated through Kruskal-Wallis tests in bioinformatics analysis, while unpaired t-tests with Welch's correction were utilized in RT-qPCR data analysis. Two-tailed tests were conducted to estimate all parametric analyses with $P< 0.05$ considered as statistical significance. All results were expressed as mean ± standard deviation.

Results

Identification of the 12 m6A modulators in PMOP

Totally 12 m6A modulators were identified based on difference analysis between controls and PMOP cases. These modulators included one eraser (FTO), five writers (METTL3, ZC3H13, RBM15B, WTAP, and RBM15), and six readers (YTHDC2, ELAVL1, FMR1, YTHDF3, HNRNPC, and IGFBP3). We finally filtrated 7 vital m6A modulators (HNRNPC, YTHDC2, FMR1, FTO, WTAP, RBM15B, and RBM15), which were visualized by a heat map and histogram. We observed that RBM15B expression was decreased in PMOP cases compared to controls, while the other significant m6A regulators displayed the opposite results (Figures 2A, C). And we visualized the chromosomal positions of the 12 m6A modulators *via* the "RCircos" package (Figure 2B).

Correlation among writers, readers and eraser in PMOP

We utilized linear regression analyses to investigate whether gene expression levels of writers or readers in PMOP exhibit correlation with the gene expression level of eraser. We observed that the gene

TABLE 2 Sequences of m6A gene-specific primers used for RT-qPCR.

m6A genes	Sequence (5′->3′)	
	Forward primer	Reverse primer
FTO	ATTCTATCAGCAGTGGCAGC	GGATGCGAGATACCGGAGTG
FMR1	CCTGAACTCAAGGCTTGGCA	TCTCTTCCTCTGTTGGAGCTTTA
YTHDC2	ACGGGGACCAGAGAGAAATG	TTGTTGAGTCGCCCACTTGT
RBM15	ATGCCTTCCCACCTTGTGAG	CAACCAGTTTTGCACGGACA
WTAP	GCTTCTGCCTGGAGAGGATT	GTGTACTTGCCCTCCAAAGC

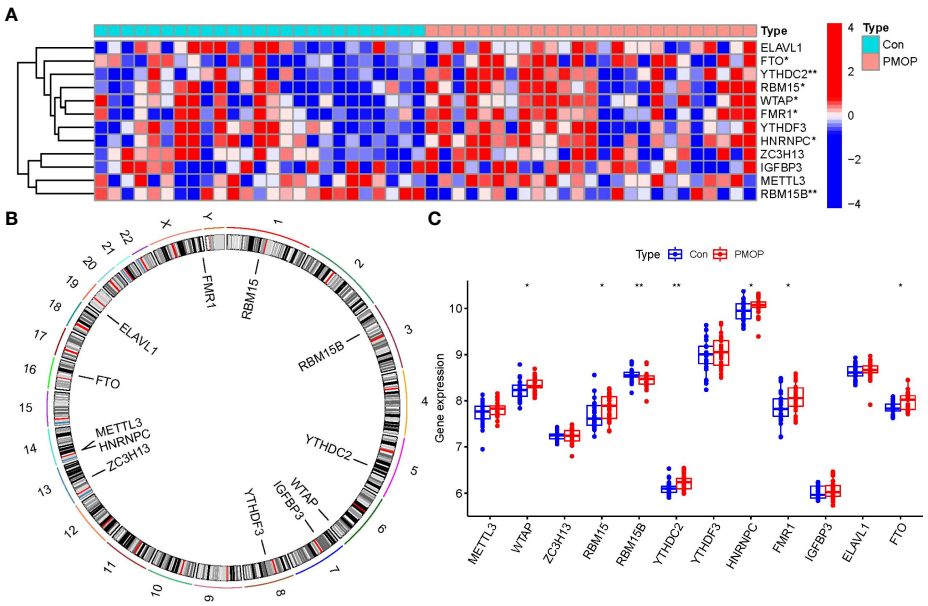

FIGURE 2
Identification of the 12 m6A modulators in PMOP. **(A)** Expression heat map of the 12 m6A modulators in controls and PMOP cases. **(B)** Chromosomal positions of the 12 m6A modulators. **(C)** Differential expression boxplots of the 12 m6A modulators between controls and PMOP cases. *p < 0.05, and **p < 0.01.

expression levels of writers RBM15, WTAP, ZC3H13, and readers FMR1, YTHDC2, and HNRNPC in PMOP cases were positively correlated with eraser gene FTO. The other readers or writers were not significantly linked to eraser gene FTO (Figure 3). Thus, we demonstrated different correlations between different writers, readers and eraser.

Establishment of the RF and SVM models

Figure 4A showed "Reverse cumulative distribution of residual" and Figure 4B presented "Boxplots of residual", which confirmed that the RF model has the smallest residuals. The residuals for most of the samples in the model are relatively small, suggesting that the RF model is better than the SVM model. Therefore, we determined the RF model to be the most suitable model for the prediction of PMOP occurrence. Then, we plotted ROC curve to estimate the models, and found that the RF model is more accurate than the SVM model according to their AUC values of the ROC curves (Figure 4C). Finally, we visualized these 7 significant m6A regulators after ranking them in order of importance and selected m6A regulators with importance score>2 as the candidate genes (Figure 4D).

Establishment of the nomogram model

We utilized the "rms" package in R to establish a nomogram model of the seven candidate m6A modulators for the prediction of the prevalence of PMOP patients (Figure 5A). We observed that the nomogram model exhibits high accuracy of prediction according to calibration curves (Figure 5B). The red line in the DCA curve stayed above the gray and black lines from 0 to 1, suggesting that decisions based on the nomogram model may be beneficial to PMOP patients (Figure 5C). Moreover, we noticed that the predictive power of the nomogram model was remarkable according to the clinical impact curve (Figure 5D).

Identification of two distinct m6A patterns

We identified two m6A patterns (clusterA and clusterB) based on the 7 significant m6A regulators *via* the R package of "ConsensusClusterPlus" (Figures 6A–D). There were 16 cases in clusterA, and 9 cases in clusterB. Then, we plotted the heat map and histogram, which clearly displayed the differential expression levels of the 7 significant m6A modulators between the two clusters. We observed that the expression levels of RBM15, WTAP, FMR1, FTO, YTHDC2, and HNRNPC in clusterA were higher than those in clusterB, while the expression level of RBM15B exhibited no significant differences between the two cluster (Figures 6E, F). The PCA results revealed that the two m6A patterns could be distinguished by 7 significant m6A modulators (Figure 6G). We screened totally 90 m6A-associated DEGs between the two m6A patterns, and we carried out GO and KEGG enrichment analyses to excavate the role of these DEGs in PMOP (Figures 6H, I). The detailed information of GO and KEGG enrichment analysis was

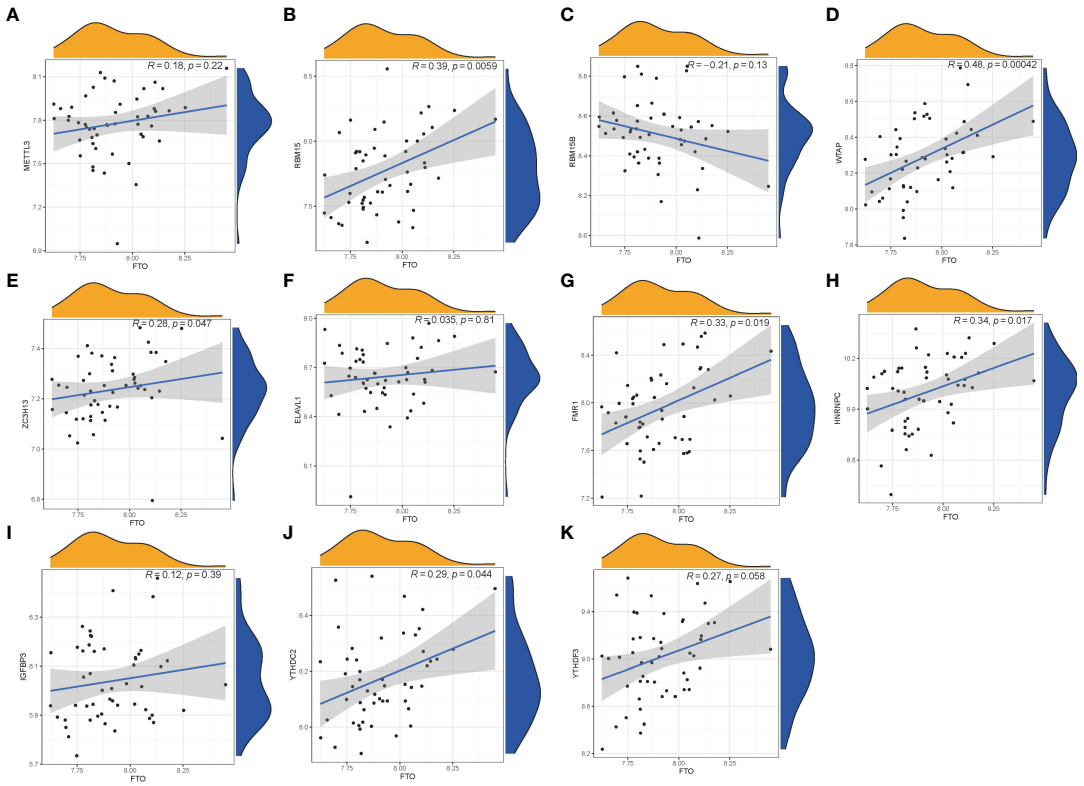

FIGURE 3
Correlation among Writers, Readers and Eraser in PMOP **(A–K)**. Writer genes: RBM15, RBM15B, METTL3, WTAP, and ZC3H13; reader genes: ELAVL1, FMR1, HNRNPC, IGFBP3, YTHDC2, and YTHDF3; eraser gene: FTO.

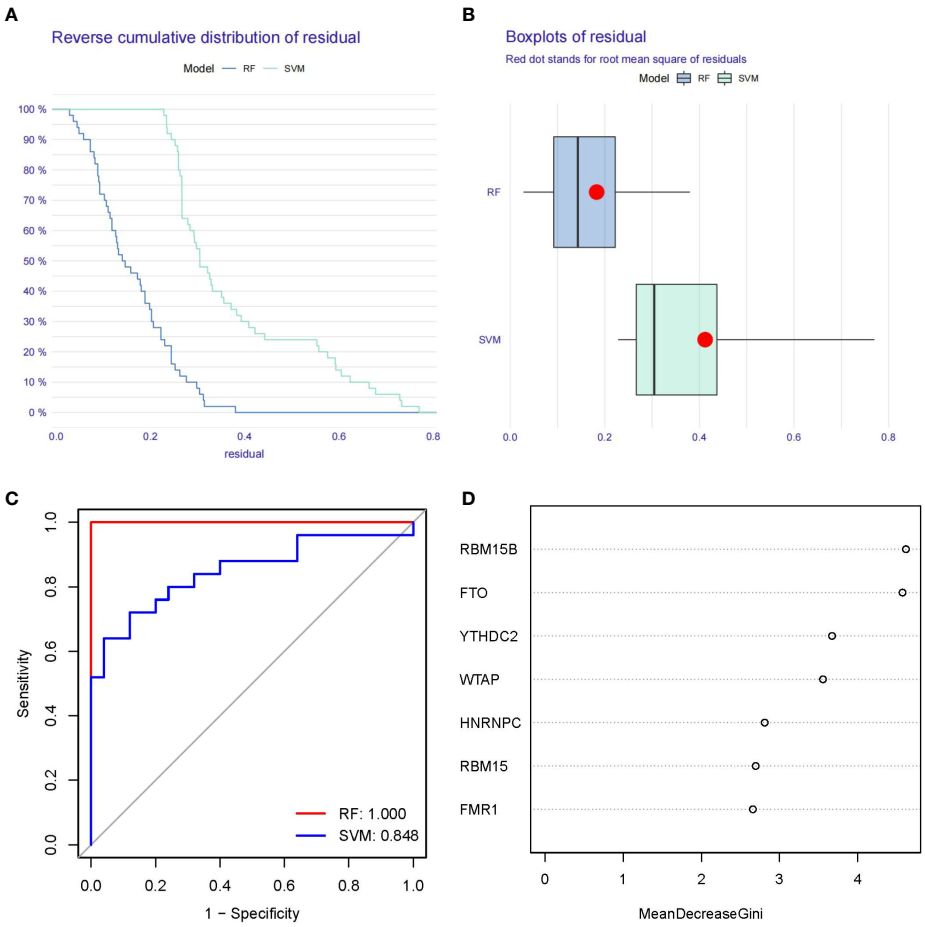

FIGURE 4
Establishment of the RF and SVM Models. **(A)** Reverse cumulative distribution of residual was constructed to display the residual distribution of RF and SVM models. **(B)** Boxplots of residual was construct to display the residual distribution of RF and SVM models. **(C)** ROC curves indicated the accuracy of the RF and SVM models. **(D)** The importance score of the 7 m6A modulators on the basis of the RF model.

shown in Supplementary Tables 1, 2. We observed that GO: 0031331 (positive regulation of cellular catabolic process), GO:0030055(cell-substrate junction), GO:0005925(focal adhesion), and GO:0045296 (cadherin binding) were the mainly enriched entries. We finally got totally 12 pathways as shown in Figure 6I. These signaling pathways like C-type lectin receptor signaling pathway, and Relaxin signaling pathway may exert regulatory functions on the pathological process of PMOP. Notably, KEGG enrichment analysis showed that osteoclast differentiation was one of the mainly enriched pathways. Specially, several key targets were involved in the pathway of osteoclast differentiation (e.g., RELB, SPI1, LILRA6, TGFB1).

Then, ssGSEA was performed to evaluate the immune cell abundance in PMOP samples, and we also assessed the correlation between immune cells and seven important m6A modulators. We observed that FMR1 was positively correlated with many immune cells (Figure 7A). We evaluated the differences in immune cell infiltration between patients with high and low FMR1 expressions. The results showed that patients with low FMR1 expression were more likely to exhibit increased immune cell infiltration than those with high FMR1 expression (Figure 7B). We found that clusterA was correlated with the immunity of immature B cell and gamma delta T cell while clusterB was related to CD56dim natural killer cell, monocyte, neutrophil and regulatory T cell immunity, indicating that clusterB may be more correlated with PMOP (Figure 7C).

Classification of two distinct m6A gene patterns and construction of the m6A gene signature

To lucubrate the m6A patterns, we used a consensus clustering approach to classify the PMOP cases into different genomic subtypes on the basis of the 90 m6A-related DEGs. We identified two distinct m6A gene patterns (gene clusterA and gene clusterB), which aligned with the sectionalization of m6A patterns (Figures 8A–D). Figure 8E displayed the expression levels of the 90 m6A-associated DEGs in gene clusterA and gene clusterB. The

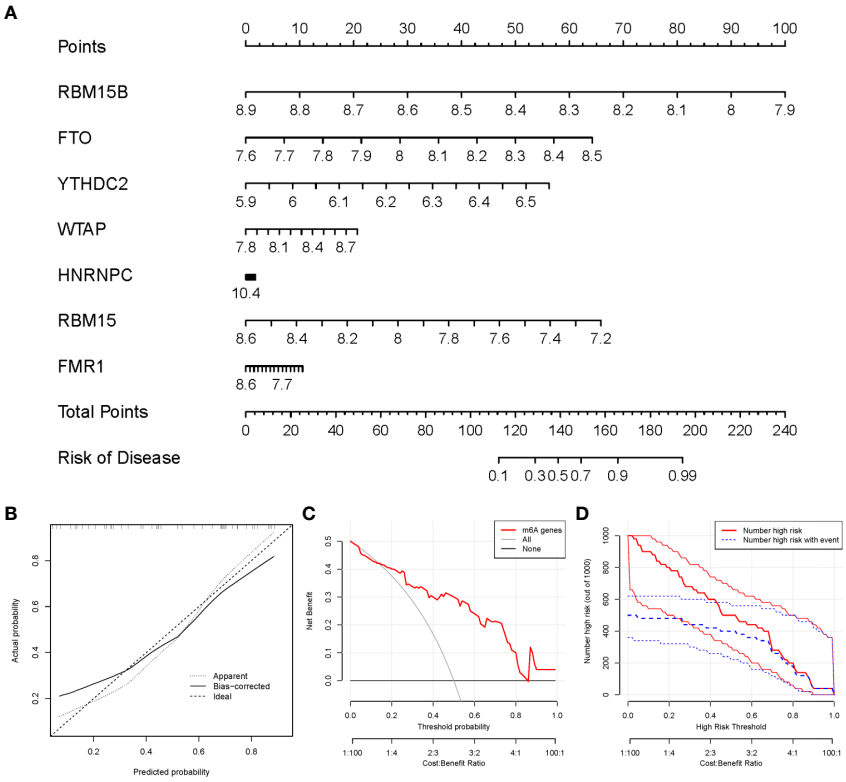

FIGURE 5
Establishment of the nomogram model. **(A)** The nomogram model was established on the basis of the 7 candidate m6A modulators. **(B)** The calibration curve was utilized to evaluate the predictive accuracy of the nomogram model. **(C)** Decisions on the basis of this nomogram model may be beneficial to PMOP patients. **(D)** The clinical impact curve was used to assess clinical impact of the nomogram model.

differential expression levels of immune cell infiltration and the 7 significant m6A modulators between gene clusterA and gene clusterB were also analogous to those in the m6A patterns (Figures 8F, G). These results again verified the veracity of our sectionalization *via* the consensus clustering approach. The m6A scores for each sample between the two distinct m6A patterns or m6A gene patterns were calculated through PCA algorithms for the quantification of the m6A patterns. We found that the clusterB or gene clusterB exhibited higher m6A score than clusterA or gene clusterA (Figures 8H, I).

Role of m6A patterns in distinguishing PMOP

We utilized a Sankey diagram to display the correlation among m6A scores, m6A patterns, and m6A gene patterns (Figure 9A). To lucubrate the link between m6A patterns and PMOP, we explored the relationship between m6A patterns and RELB, SPI1, LILRA6, and TGFB1, which were enriched in osteoclast differentiation according to KEGG enrichment analysis. We observed that clusterB or gene clusterB displayed higher expression levels of RELB, SPI1, LILRA6, and TGFB1 than clusterA or gene clusterA, indicating that clusterB or gene clusterB were closely correlated with PMOP characterized by osteoclast differentiation (Figures 9B, C).

RT-qRCR validation of significant m6A modulators

It was verified that m6A genes FTO, FMR1, YTHDC2, RBM15, WTAP exhibited significantly higher expression levels in PMOP cases than controls (Figure 10), which was consistent with the bioinformatics results.

Discussion

PMOP is a widespread musculoskeletal disorder accompanied by bone system symptoms in postmenopausal women (37). Existing researches have confirmed that m6A modulators play an indispensable role in numerous biological processes (38). However, the role of m6A rmodulators in PMOP stays unclear. This present study aimed at investigating the role of m6A modulators in PMOP.

Firstly, a total of 7 significant m6A modulators were screened from 12 m6A modulators *via* differential expression analysis between controls and PMOP cases, which were selected as diagnostic m6A modulators (FMR1, WTAP, YTHDC2, HNRNPC, FTO, RBM15, and RBM15B) based on an established RF model to predict the occurrence of PMOP. Then, we established a nomogram model on the basis of the seven candidate m6A modulators, which has been evaluated *via* the DCA curve to produce benefit to PMOP patients in virtue of decisions based on the nomogram model.

10.3389/fendo.2023.990078

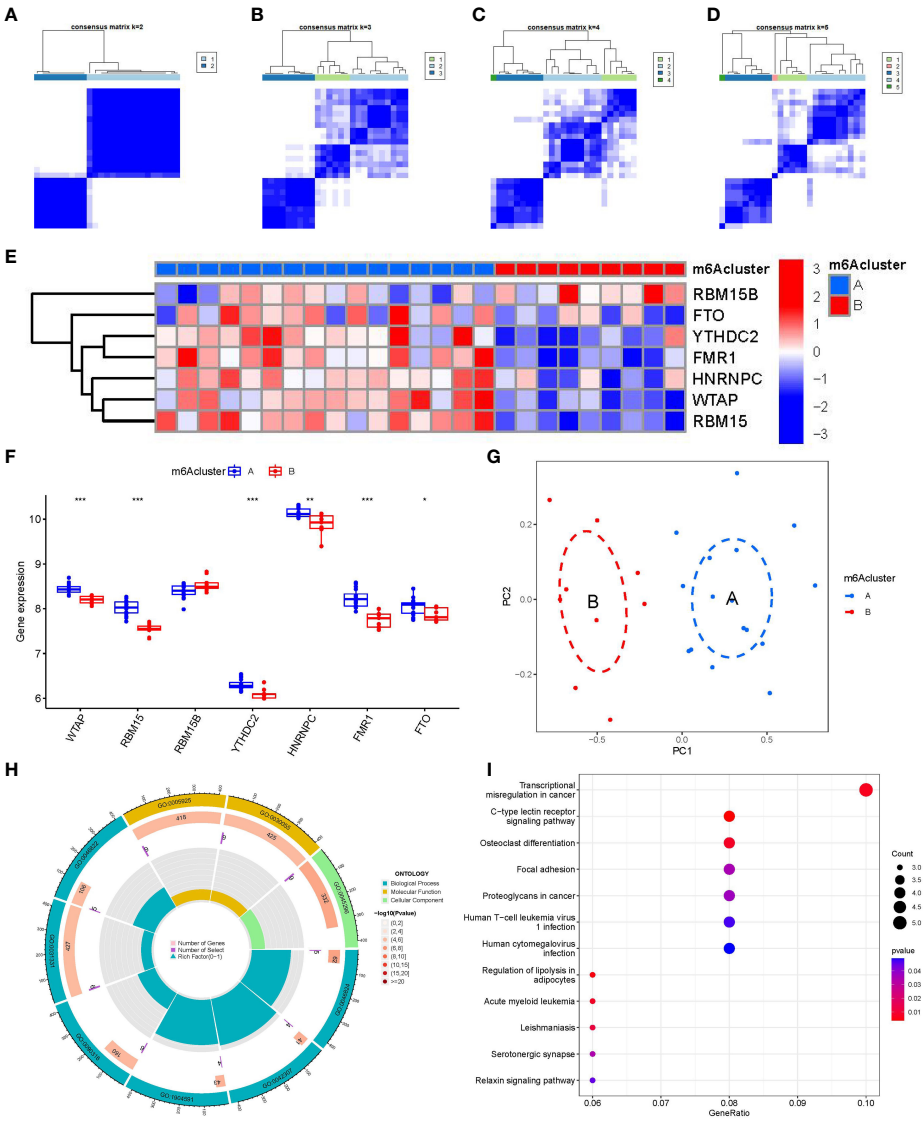

FIGURE 6
Consensus clustering of the 7 significant m6A modulators in PMOP. **(A–D)** Consensus matrices of the 7 significant m6A modulators for k = 2–5. **(E)** Expression heat map of the 7 significant m6A modulators in clusterA and clusterB. **(F)** Differential expression boxplots of the 7 significant m6A modulators in clusterA and clusterB. **(G)** Principal component analysis for the expression profiles of the 7 significant m6Amodulators that shows a remarkable difference in transcriptomes between the two m6A patterns. **(H, I)** GO and KEGG analysis that explores the potential mechanism underlying the effect of the 90 m6A-related DEGs on the occurrence and development of PMOP. *p < 0.05, **p < 0.01, and ***p < 0.001.

FMR1 encodes an RNA-binding protein FMRP, which maintains mRNA stability by binding to the m6A site of mRNA (39). Existing study has confirmed that FMR1-deficiency affects skeleton and bone microstructure, demonstrating that knock-out (KO) of FMR1 in mice showed increased femoral cortical thickness, reduced cortical eccentricity, decreased femoral trabecular pore volumes, and a higher range of trabecular thickness distribution compared to controls (40). WTAP (Wilm's tumor 1 protein) is a ubiquitous nuclear protein that has been reported to facilitate the formation of m6A (41). In addition, existing evidence has confirmed that the WTAP expression level was remarkably upregulated 7 days after fracture (42). Moreover, the increased expression of WTAP has been reported to promote cellular senescence in aging-related diseases (43). YTHDC2 belongs to the DExD/H box RNA helicase family, which exerts important functions in regulating the transcription of mRNA and maintaining the stability of mRNA (44). YTHDC2 knockdown can exert a stimulative effect on the osteogenic differentiation of human BMSCs and suppress the adipogenic differentiation (45). As a DNA binding protein, HNRNPC (Heterogeneous nuclear ribonucleoprotein C) plays an essential part in RNA processing, exerting a remarkably suppressive effect on the transcription of the vitamin D hormone,1,25-dihydroxyvitamin D (1,25(OH)2D) (46). And HNRNPC has properties of species-specific heterodimerization that functions as

10.3389/fendo.2023.990078

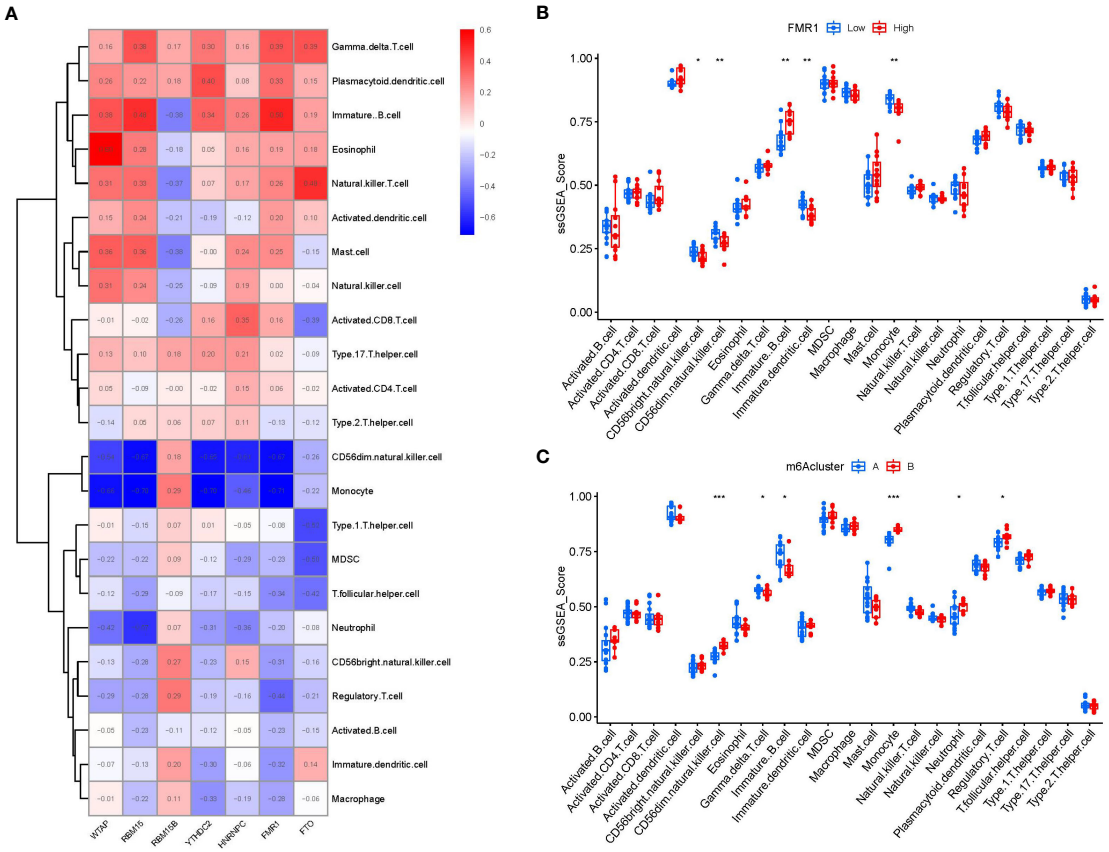

FIGURE 7
Single sample gene set enrichment analysis. **(A)** Correlation between immune cell infiltration and the 7 significant m6A modulators. **(B)** Difference in the abundance of infiltrating immune cells between high and low FMR1 protein expression groups. **(C)** Differential immune cell infiltration between clusterA and clusterB. *p < 0.05, **p < 0.01, and ***p < 0.001.

an indispensable prerequisite for DNA binding and down-regulation of 1,25(OH)2D-related gene transactivation in osteoblasts (47). FTO is a primary m6A demethylase that suppresses osteogenic differentiation by demethylating runx2 mRNA, thus accelerating the process of osteoporosis (48). It has also been found that FTO is a regulator that determines the differentiation of BMSCs by affecting the activation of the GDF11 signaling axis in the bone marrow, promoting Smad2/3 phosphorylation to stimulate osteoclastogenesis and inhibit osteoblast differentiation, thus leading to the development of osteoporosis (49–51). The RNA binding motif protein 15 (RBM15/OTT1) and its paralogue RBM15B (OTT3) belong to SPEN family members (52). Existing studies have confirmed that RBM15 in stress hematopoiesis have a variety of aging-related physiologic changes, including increased DNA damage and NF-κB activation (53), which may serve as important pathological factors in the development of osteoporosis. In addition, study has reported that knockdown of RBM15 and RBM15B impairs XIST-mediated gene silencing (52), which influences osteoblast differentiation in osteoporosis (54). Therefore, to our knowledge, the seven candidate m6A modulators may play an important part in the occurrence and development of osteoporosis according to previous studies.

Existing researches reveal that the dysfunction of T and B ymphocytes may play an essential role in the pathogenesis of PMOP (55). We found that clusterA was correlated with the immunity of immature B cell and gamma delta T cell while clusterB was related to CD56dim natural killer cell, monocyte, neutrophil and regulatory T cell immunity, indicating that clusterB may be more correlated with PMOP (Figure 7C). Regulatory T cell (Treg) exerts an essential regulatory function in maintaining immune homeostasis and inhibiting the evolution of PMOP (56). Treg cells negatively regulate osteoclasts in bone metabolism, inhibiting osteoclast formation and differentiation and reducing osteoclast activity (57). The immune and skeletal systems share many regulatory factors, such as transforming growth factor-β (TGFB1), which inhibits osteoclast function of bone resorption and regulates new bone formation in bone resorption region (58). Bozec et al (59) found that Treg cells can regulate osteoclastogenesis by secreting cytokines such as TGFB1, IL-10 and IL-4. In this study, we identified two distinct m6A patterns (clusterA and clusterB) on the basis of the 7 significant m6A modulators as well as two distinct m6A gene patterns

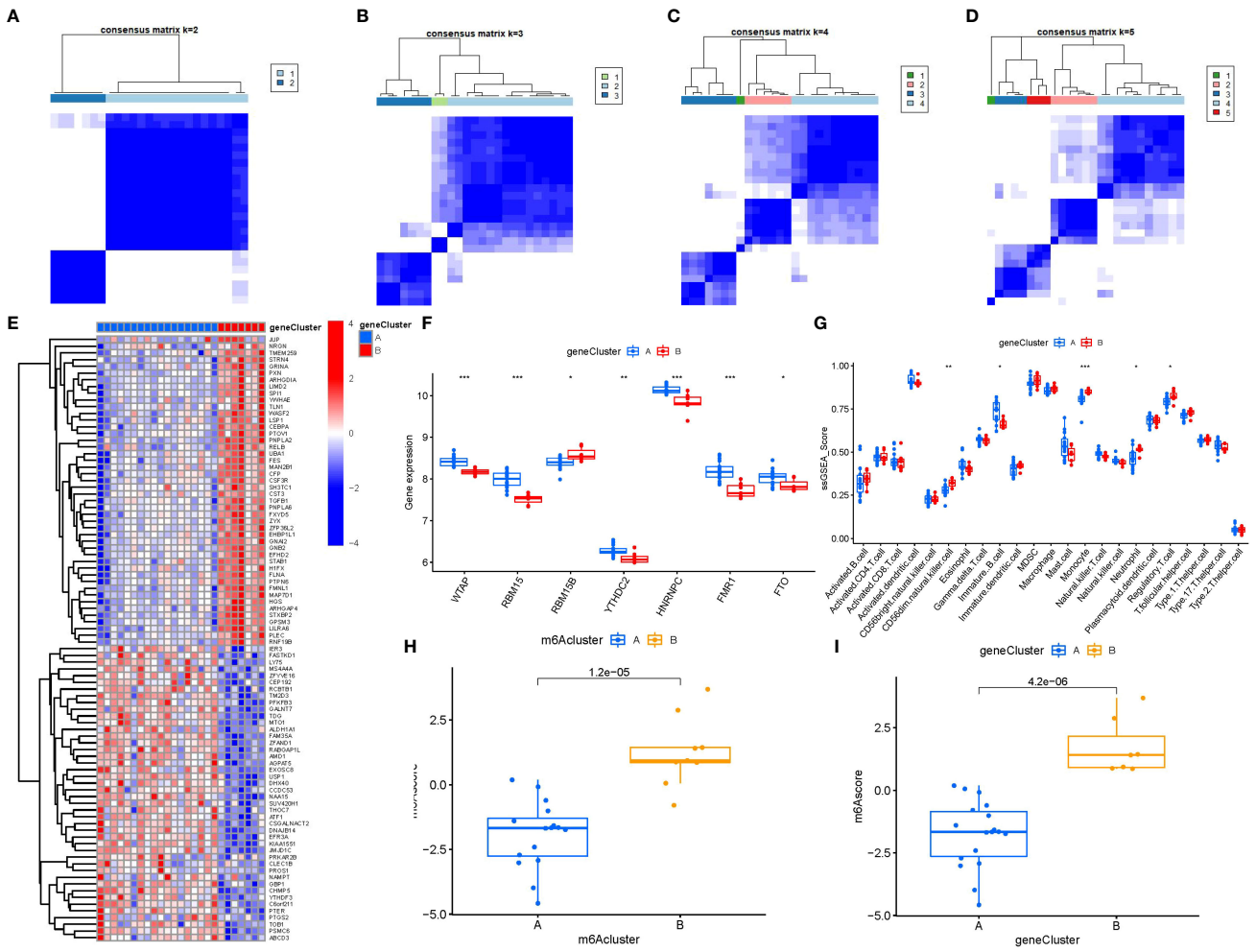

FIGURE 8
Consensus clustering of the 90 m6A-associated DEGs in PMOP. **(A–D)** Consensus matrices of the 90 m6A-associated DEGs for k = 2–5. **(E)** Expression heat map of the 90 m6A-associated DEGs in gene clusterA and gene clusterB. **(F)** Differential expression boxplots of the 7 significant m6A modulators in gene clusterA and gene clusterB. **(G)** Differential immune cell infiltration between gene clusterA and gene clusterB. **(H)** Differences in m6A score between clusterA and clusterB. **(I)** Differences in m6A score between gene clusterA and gene clusterB. *p < 0.05, **p < 0.01, and ***p < 0.001.

(gene clusterA and gene clusterB) based on the 90 m6A-associated DEGs. RELB, SPI1, LILRA6, and TGFB1 were enriched in the pathway of osteoclast differentiation according to KEGG enrichment analysis of the 90 m6A-associated DEGs. ClusterB was closely correlated with the regulatory T cell (Treg) immunity and displayed higher expression levels of RELB, SPI1, LILRA6, and TGFB1, suggesting that clusterB may be linked to osteoclast differentiation. Moreover, the m6A scores for each sample between the two distinct m6A patterns or m6A gene patterns were calculated through PCA algorithms for the quantification of the m6A patterns. We found that the clusterB or gene clusterB exhibited higher m6A score than clusterA or gene clusterA.

Our RT-qPCR experiments verified that m6A genes FTO, FMR1, YTHDC2, RBM15, WTAP exhibited significantly higher expression levels in PMOP cases than controls (Figure 10), which was consistent with the bioinformatics results and previous studies. Our results confirm the involvement of these m6A regulators in PMOP and provide new clues to their role in the pathogenesis of PMOP, which further verified the possibility that m6A modulators may play an important role in the development of PMOP. To the best of our knowledge, this study is the first time to report m6A-related diagnostic biomarkers of PMOP in the subtype classification of blood monocytes.

However, there remain some limitations in our study. This study analyzed the relationship between m6A regulators and immune cell infiltration and briefly validated the expression of key m6A regulators in the samples from PMOP patients, but the underlying regulatory mechanisms in the progression of PMOP have not yet been fully elucidated. In the future, more *in vivo*, *in vitro* and clinical experiments are needed to verify the bioinformatics results.

Conclusion

In general, our present study screened seven diagnostic m6A modulators and constructed a nomogram model providing accurate

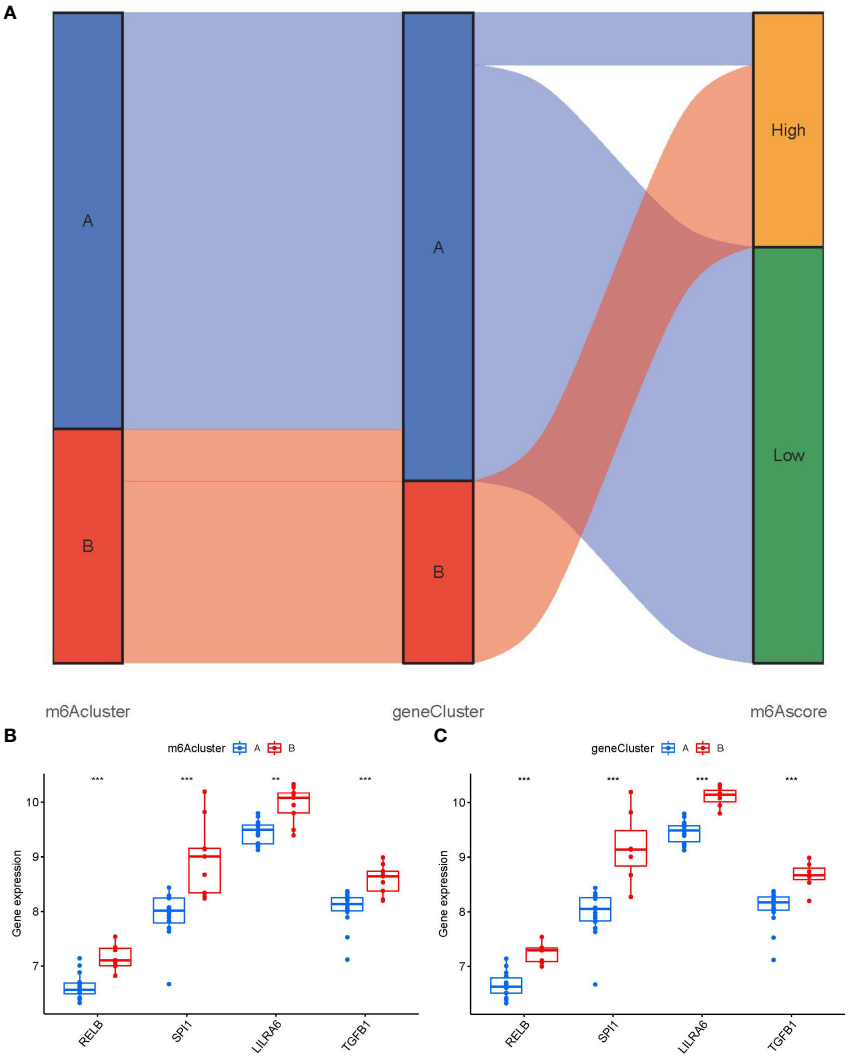

FIGURE 9
Role of m6A patterns in distinguishing PMOP. **(A)** Sankey diagram showing the relationship between m6A patterns, m6A gene patterns, and m6A scores. **(B)** Differential expression levels of osteoclast differentiation-related genes between clusterA and clusterB. **(C)** Differential expression levels of osteoclast differentiation-related genes between gene clusterA and gene clusterB. **p < 0.01, and ***p < 0.001.

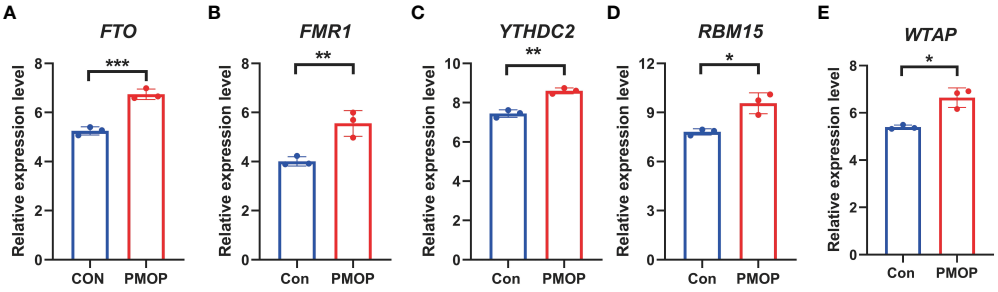

FIGURE 10
RT-qPCR experimental validation of significant m6A modulators. **(A–E)** Relative mRNA expressions of 5 key m6A modulators including FTO, FMR1, YTHDC2, RBM15 and WTAP between the two groups. All results were expressed as mean ± standard deviation. *p < 0.05, **p < 0.01, and ***p < 0.001.

prediction for the prevalence of PMOP. Then, we authenticatd two m6A patterns based on the 7 m6A modulator, and found that clusterB may be more correlated with PMOP. To our knowledge, this study is the first to report m6A-related diagnostic biomarkers of PMOP in the subtype classification of blood monocytes.

Data availability statement

The datasets presented in this study can be found in online repositories. The names of the repository/repositories and accession number(s) can be found in the article/Supplementary Material.

Ethics statement

The clinical experiments involved in this paper were authorized by the Ethics Committee of the First Affiliated Hospital of Guangzhou University of Chinese Medicine (No. K[2019]129). The patients/participants provided their written informed consent to participate in this study.

Author contributions

PZ, HC, DL, JT, JC, ZL, HR, and XJ contributed to the study conception and design. PZ, HC, BX, WZ, and QS contributed to the bioinformatics analysis and experimental validation. JH, GS, XY, ZZ, GZ, GC, and FY contributed to data analysis, and drafting the manuscript. All authors contributed to the article and approved the submitted version.

Funding

The project was generously supported by the grants from National Natural Science Foundation of China (82274542, 82274615, 81904225, 82205137 and 82205230), Guangdong Natural Science Foundation (2022A1515012062 and 2021A1515011247), Innovative Team Project and Key Project of the Department of Education of Guangdong Province (2021KCXTD017), High-Level University Collaborative Innovation Team of Guangzhou University of Chinese Medicine (2021xk57), Medical Research Foundation of Guangdong Province (A2021320), Guangzhou Science and Technology Project (202201020307), Scientific Research Project of Excellent Young Scholars Project of First Affiliated Hospital of Guangzhou University of Chinese Medicine (2019QN17), Scientific Research Project of Traditional Chinese Medicine Bureau of Guangdong Province (20201097 and 20221308). The funding institutions had not any role in the study design, data collection, data analysis, interpretation, or writing of the report in this study.

Acknowledgments

We show gratitude for the authors who provided the GEO public datasets.

Conflict of interest

The authors declare that the research was conducted in the absence of any commercial or financial relationships that could be construed as a potential conflict of interest.

Publisher's note

Supplementary material

The Supplementary Material for this article can be found online at: https://www.frontiersin.org/articles/10.3389/fendo.2023.990078/full#supplementary-material

References

1. Arceo-Mendoza RM, Camacho PM. Postmenopausal osteoporosis: Latest guidelines. *Endocrinol Metab Clin North Am* (2021) 50(2):167–78. doi: 10.1016/j.ecl.2021.03.009

2. Slupski W, Jawien P, Nowak B. Botanicals in postmenopausal osteoporosis. *Nutrients* (2021) 13(5). doi: 10.3390/nu13051609

3. Huidrom S, Beg MA, Masood T. Post-menopausal osteoporosis and probiotics. *Curr Drug Targets* (2021) 22(7):816–22. doi: 10.2174/1389450121666201027124947

4. Reid IR. A broader strategy for osteoporosis interventions. *Nat Rev Endocrinol* (2020) 16(6):333–9. doi: 10.1038/s41574-020-0339-7

5. Tian A, Jia H, Zhu S, Lu B, Li Y, Ma J, et al. Romosozumab versus teriparatide for the treatment of postmenopausal osteoporosis: A systematic review and meta-analysis through a grade analysis of evidence. *Orthop Surg* (2021) 13(7):1941–50. doi: 10.1111/os.13136

6. Han J, Li L, Zhang C, Huang Q, Wang S, Li W, et al. Eucommia, cuscuta, and drynaria extracts ameliorate glucocorticoid-induced osteoporosis by inhibiting osteoclastogenesis through PI3K/Akt pathway. *Front Pharmacol* (2021) 12:772944. doi: 10.3389/fphar.2021.772944

7. McNeil MA, Merriam SB. Menopause. *Ann Intern Med* (2021) 174(7):ITC97–ITC112. doi: 10.7326/AITC202107200

8. Si L, Winzenberg TM, Jiang Q, Chen M, Palmer AJ. Projection of osteoporosis-related fractures and costs in China: 2010-2050. *Osteoporos Int* (2015) 26(7):1929–37. doi: 10.1007/s00198-015-3093-2

9. Yin L, Zhu X, Novak P, Zhou L, Gao L, Yang M, et al. The epitranscriptome of long noncoding RNAs in metabolic diseases. *Clin Chim Acta* (2021) 515:80–9. doi: 10.1016/j.cca.2021.01.001

10. Dong Q, Han Z, Tian L. Identification of serum exosome-derived circRNA-miRNA-TF-mRNA regulatory network in postmenopausal osteoporosis using bioinformatics analysis and validation in peripheral blood-derived mononuclear cells. *Front Endocrinol (Lausanne)* (2022) 13:899503. doi: 10.3389/fendo.2022.899503

11. Cui Y, Guo Y, Kong L, Shi J, Liu P, Li R, et al. A bone-targeted engineered exosome platform delivering siRNA to treat osteoporosis. *Bioact Mater* (2022) 10:207–21. doi: 10.1016/j.bioactmat.2021.09.015

12. Kalluri R, LeBleu VS. The biology, function, and biomedical applications of exosomes. *Science* (2020) 367(6478). doi: 10.1126/science.aau6977

13. Jeppesen DK, Fenix AM, Franklin JL, Higginbotham JN, Zhang Q, Zimmerman LJ, et al. Reassessment of exosome composition. *Cell* (2019) 177(2):428–445 e418. doi: 10.1016/j.cell.2019.02.029

14. Pegtel DM, Gould SJ. Exosomes. *Annu Rev Biochem* (2019) 88:487–514. doi: 10.1146/annurev-biochem-013118-111902

15. Liu Z, Li C, Huang P, Hu F, Jiang M, Xu X, et al. CircHmbox1 targeting miRNA-1247-5p is involved in the regulation of bone metabolism by TNF-alpha in postmenopausal osteoporosis. *Front Cell Dev Biol* (2020) 8:594785. doi: 10.3389/fcell.2020.594785

16. Xu T, He B, Sun H, Xiong M, Nie J, Wang S, et al. Novel insights into the interaction between N6-methyladenosine modification and circular RNA. *Mol Ther Nucleic Acids* (2022) 27:824–37. doi: 10.1016/j.omtn.2022.01.007

17. Yang Y, Hsu PJ, Chen YS, Yang YG. Dynamic transcriptomic m(6)A decoration: writers, erasers, readers and functions in RNA metabolism. *Cell Res* (2018) 28(6):616–24. doi: 10.1038/s41422-018-0040-8

18. Zhang N, Ding C, Zuo Y, Peng Y, Zuo L. N6-methyladenosine and neurological diseases. *Mol Neurobiol* (2022) 59(3):1925–37. doi: 10.1007/s12035-022-02739-0

19. Meng L, Lin H, Huang X, Weng J, Peng F, Wu S. METTL14 suppresses pyroptosis and diabetic cardiomyopathy by downregulating TINCR lncRNA. *Cell Death Dis* (2022) 13(1):38. doi: 10.1038/s41419-021-04484-z

20. Liu T, Zheng X, Wang C, Wang C, Jiang S, Li B, et al. The m(6)A "reader" YTHDF1 promotes osteogenesis of bone marrow mesenchymal stem cells through translational control of ZNF839. *Cell Death Dis* (2021) 12(11):1078. doi: 10.1038/s41419-021-04312-4

21. Huang M, Xu S, Liu L, Zhang M, Guo J, Yuan Y, et al. m6A methylation regulates osteoblastic differentiation and bone remodeling. *Front Cell Dev Biol* (2021) 9:783322. doi: 10.3389/fcell.2021.783322

22. Chen S, Li Y, Zhi S, Ding Z, Wang W, Peng Y, et al. WTAP promotes osteosarcoma tumorigenesis by repressing HMBOX1 expression in an m(6)A-dependent manner. *Cell Death Dis* (2020) 11(8):659. doi: 10.1038/s41419-020-02847-6

23. Zhang Y, Liang C, Wu X, Pei J, Guo X, Chu M, et al. Integrated study of transcriptome-wide m(6)A methylome reveals novel insights into the character and function of m(6)A methylation during yak adipocyte differentiation. *Front Cell Dev Biol* (2021) 9:689067. doi: 10.3389/fcell.2021.689067

24. Chen X, Gong W, Shao X, Shi T, Zhang L, Dong J, et al. METTL3-mediated m(6)A modification of ATG7 regulates autophagy-GATA4 axis to promote cellular senescence and osteoarthritis progression. *Ann Rheum Dis* (2022) 81(1):87–99. doi: 10.1136/annrheumdis-2021-221091

25. Wu Y, Xie L, Wang M, Xiong Q, Guo Y, Liang Y, et al. Mettl3-mediated m(6)A RNA methylation regulates the fate of bone marrow mesenchymal stem cells and osteoporosis. *Nat Commun* (2018) 9(1):4772. doi: 10.1038/s41467-018-06898-4

26. Sun Z, Wang H, Wang Y, Yuan G, Yu X, Jiang H, et al. MiR-103-3p targets the m (6) a methyltransferase METTL14 to inhibit osteoblastic bone formation. *Aging Cell* (2021) 20(2):e13298. doi: 10.1111/acel.13298

27. Zhou Y, Gao Y, Xu C, Shen H, Tian Q, Deng HW. A novel approach for correction of crosstalk effects in pathway analysis and its application in osteoporosis research. *Sci Rep* (2018) 8(1):668. doi: 10.1038/s41598-018-19196-2

28. Liu YZ, Dvornyk V, Lu Y, Shen H, Lappe JM, Recker RR, et al. A novel pathophysiological mechanism for osteoporosis suggested by an *in vivo* gene expression study of circulating monocytes. *J Biol Chem* (2005) 280(32):29011–6. doi: 10.1074/jbc.M501164200

29. Ritchie ME, Phipson B, Wu D, Hu Y, Law CW, Shi W, et al. Limma powers differential expression analyses for RNA-sequencing and microarray studies. *Nucleic Acids Res* (2015) 43(7):e47. doi: 10.1093/nar/gkv007

30. Bao X, Shi R, Zhao T, Wang Y. Mast cell-based molecular subtypes and signature associated with clinical outcome in early-stage lung adenocarcinoma. *Mol Oncol* (2020) 14 (5):917–32. doi: 10.1002/1878-0261.12670

31. Dai B, Sun F, Cai X, Li C, Liu H, Shang Y. Significance of RNA N6-methyladenosine regulators in the diagnosis and subtype classification of childhood asthma using the gene expression omnibus database. *Front Genet* (2021) 12:634162. doi: 10.3389/fgene.2021.634162

32. Wilkerson MD, Hayes DN. ConsensusClusterPlus: A class discovery tool with confidence assessments and item tracking. *Bioinformatics* (2010) 26(12):1572–3. doi: 10.1093/bioinformatics/btq170

33. Denny P, Feuermann M, Hill DP, Lovering RC, Plun-Favreau H, Roncaglia P. Exploring autophagy with gene ontology. *Autophagy* (2018) 14(3):419–36. doi: 10.1080/15548627.2017.1415189

34. Zhang B, Wu Q, Li B, Wang D, Wang L, Zhou YL. m(6)A regulator-mediated methylation modification patterns and tumor microenvironment infiltration characterization in gastric cancer. *Mol Cancer* (2020) 19(1):53. doi: 10.1186/s12943-020-01170-0

35. Zhang N, Zhao YD, Wang XM. CXCL10 an important chemokine associated with cytokine storm in COVID-19 infected patients. *Eur Rev Med Pharmacol Sci* (2020) 24 (13):7497–505. doi: 10.26355/eurrev_202007_21922

36. Chen H, Shen G, Shang Q, Zhang P, Yu D, Yu X, et al. Plastrum testudinis extract suppresses osteoclast differentiation *via* the NF-kappaB signaling pathway and ameliorates senile osteoporosis. *J Ethnopharmacol* (2021) 276:114195. doi: 10.1016/j.jep.2021.114195

37. Eastell R, Szulc P. Use of bone turnover markers in postmenopausal osteoporosis. *Lancet Diabetes Endocrinol* (2017) 5(11):908–23. doi: 10.1016/S2213-8587(17)30184-5

38. Oerum S, Meynier V, Catala M, Tisne C. A comprehensive review of m6A/m6Am RNA methyltransferase structures. *Nucleic Acids Res* (2021) 49(13):7239–55. doi: 10.1093/nar/gkab378

39. Zhang F, Kang Y, Wang M, Li Y, Xu T, Yang W, et al. Fragile X mental retardation protein modulates the stability of its m6A-marked messenger RNA targets. *Hum Mol Genet* (2018) 27(22):3936–50. doi: 10.1093/hmg/ddy292

40. Leboucher A, Bermudez-Martin P, Mouska X, Amri EZ, Pisani DF, Davidovic L. Fmr1-deficiency impacts body composition, skeleton, and bone microstructure in a mouse model of fragile X syndrome. *Front Endocrinol (Lausanne)* (2019) 10:678. doi: 10.3389/fendo.2019.00678

41. Zhang SY, Zhang SW, Liu L, Meng J, Huang Y. m6A-driver: Identifying context-specific mRNA m6A methylation-driven gene interaction networks. *PloS Comput Biol* (2016) 12(12):e1005287. doi: 10.1371/journal.pcbi.1005287

42. Mi B, Xiong Y, Yan C, Chen L, Xue H, Panayi AC, et al. Methyltransferase-like 3-mediated N6-methyladenosine modification of miR-7212-5p drives osteoblast differentiation and fracture healing. *J Cell Mol Med* (2020) 24(11):6385–96. doi: 10.1111/jcmm.15284

43. Li G, Ma L, He S, Luo R, Wang B, Zhang W, et al. WTAP-mediated m(6)A modification of lncRNA NORAD promotes intervertebral disc degeneration. *Nat Commun* (2022) 13(1):1469. doi: 10.1038/s41467-022-28990-6

44. He JJ, Li Z, Rong ZX, Gao J, Mu Y, Guan YD, et al. m(6)A reader YTHDC2 promotes radiotherapy resistance of nasopharyngeal carcinoma *via* activating IGF1R/AKT/S6 signaling axis. *Front Oncol* (2020) 10:1166. doi: 10.3389/fonc.2020.01166

45. Wen JR, Tan Z, Lin WM, Li QW, Yuan Q. [Role of m (6)A reader YTHDC2 in differentiation of human bone marrow mesenchymal stem cells]. *Sichuan Da Xue Xue Bao Yi Xue Ban* (2021) 52(3):402–8. doi: 10.12182/20210560204

46. Zhou R, Park JW, Chun RF, Lisse TS, Garcia AJ, Zavala K, et al. Concerted effects of heterogeneous nuclear ribonucleoprotein C1/C2 to control vitamin d-directed gene transcription and RNA splicing in human bone cells. *Nucleic Acids Res* (2017) 45(2):606–18. doi: 10.1093/nar/gkw851

47. Lisse TS, Vadivel K, Bajaj SP, Chun RF, Hewison M, Adams JS. The heterodimeric structure of heterogeneous nuclear ribonucleoprotein C1/C2 dictates 1,25-dihydroxyvitamin d-directed transcriptional events in osteoblasts. *Bone Res* (2014) 2. doi: 10.1038/boneres.2014.11

48. Wang J, Fu Q, Yang J, Liu JL, Hou SM, Huang X, et al. RNA N6-methyladenosine demethylase FTO promotes osteoporosis through demethylating Runx2 mRNA and inhibiting osteogenic differentiation. *Aging (Albany NY)* (2021) 13(17):21134–41. doi: 10.18632/aging.203377

49. Jin M, Song S, Guo L, Jiang T, Lin ZY. Increased serum GDF11 concentration is associated with a high prevalence of osteoporosis in elderly native Chinese women. *Clin Exp Pharmacol Physiol* (2016) 43(11):1145–7. doi: 10.1111/1440-1681.12651

50. Lu Q, Tu ML, Li CJ, Zhang L, Jiang TJ, Liu T, et al. GDF11 inhibits bone formation by activating Smad2/3 in bone marrow mesenchymal stem cells. *Calcif Tissue Int* (2016) 99(5):500–9. doi: 10.1007/s00223-016-0173-z

51. Liu W, Zhou L, Zhou C, Zhang S, Jing J, Xie L, et al. GDF11 decreases bone mass by stimulating osteoclastogenesis and inhibiting osteoblast differentiation. *Nat Commun* (2016) 7:12794. doi: 10.1038/ncomms12794

52. Patil DP, Chen CK, Pickering BF, Chow A, Jackson C, Guttman M, et al. m(6)A RNA methylation promotes XIST-mediated transcriptional repression. *Nature* (2016) 537 (7620):369–73. doi: 10.1038/nature19342

53. Xiao N, Jani K, Morgan K, Okabe R, Cullen DE, Jesneck JL, et al. Hematopoietic stem cells lacking Ott1 display aspects associated with aging and are unable to maintain quiescence during proliferative stress. *Blood* (2012) 119(21):4898–907. doi: 10.1182/blood-2012-01-403089

54. Chen X, Ma F, Zhai N, Gao F, Cao G. Long noncoding RNA XIST inhibits osteoblast differentiation and promotes osteoporosis *via* Nrf2 hyperactivation by targeting CUL3. *Int J Mol Med* (2021) 48(1). doi: 10.3892/ijmm.2021.4970

55. Brunetti G, Storlino G, Oranger A, Colaianni G, Faienza MF, Ingravallo G, et al. LIGHT/TNFSF14 regulates estrogen deficiency-induced bone loss. *J Pathol* (2020) 250 (4):440–51. doi: 10.1002/path.5385

56. Bhadricha H, Patel V, Singh AK, Savardekar L, Patil A, Surve S, et al. Increased frequency of Th17 cells and IL-17 levels are associated with low bone mineral density in postmenopausal women. *Sci Rep* (2021) 11(1):16155. doi: 10.1038/s41598-021-95640-0

57. Zhu L, Hua F, Ding W, Ding K, Zhang Y, Xu C. The correlation between the Th17/Treg cell balance and bone health. *Immun Ageing* (2020) 17:30. doi: 10.1186/s12979-020-00202-z

58. Lee B, Oh Y, Jo S, Kim TH, Ji JD. A dual role of TGF-beta in human osteoclast differentiation mediated by Smad1 versus Smad3 signaling. *Immunol Lett* (2019) 206:33–40. doi: 10.1016/j.imlet.2018.12.003

59. Bozec A, Zaiss MM. T Regulatory cells in bone remodelling. *Curr Osteoporos Rep* (2017) 15(3):121–5. doi: 10.1007/s11914-017-0356-1